THE ASTROPHYSICAL JOURNAL, 519:291–302, 1999 July 1

MODEL FOR DETERMINISTIC CHAOS IN PULSAR RADIO SIGNALS AND SEARCH FOR ATTRACTORS IN THE CRAB AND VELA PULSARS

TRACEY DELANEY[1] AND JAMES C. WEATHERALL
Department of Physics, New Mexico Institute of Mining and Technology, Socorro, NM 87801; tdelaney@ast1.spa.umn.edu, jweather@aoc.nrao.edu
Received 1998 March 23; accepted 1999 February 1

ABSTRACT

We search for evidence of a chaotic attractor in data from the Vela and Crab pulsars and in a coherent turbulent plasma model for pulsar emission. Both the model and the observational data are tested using the method of time delays to reconstruct an attractor and the method of Grassberger & Procaccia to compute its dimension. The analysis is an attempt to compare theory with observation. The plasma model clearly shows a low-dimensional attractor; this result is confirmed by computing the largest Lyapunov exponent. There is no evidence for chaos in any of the pulsar data. A definitive test will require pulsar data of extremely high time resolution.

Subject headings: chaos — pulsars: general — pulsars: individual (Crab pulsar, Vela pulsar) — radiation mechanisms: nonthermal — turbulence

1. INTRODUCTION

Deterministic chaos is the unpredictable and apparently random behavior exhibited by certain systems even though those systems are governed by fully deterministic laws. Chaos is characterized by a sensitive dependence on initial conditions and a strange attractor in the phase space of the system. An attractor is the path that a trajectory in phase space tends to follow. When phase-space trajectories have a strange attractor, simple orbits do not close on themselves and appear distorted into never repeating loops of a fractal-like structure. A strange attractor is characterized by a non-integer dimension. To measure the dimension of an attractor, the correlation sum method of Grassberger & Procaccia (1983) is frequently used. For those instances when the phase space of the system is not known, it is useful to apply the method of time delays (Packard et al. 1980; Takens 1981). This is true for pulsar radio data, which consist only of a time series of information about the system generating the emission. The method of time delays enables the attractor to be reconstructed from delay vectors derived from the time series; then the dimension of the reconstructed attractor can be computed by the Grassberger & Procaccia method.

When necessary, the Grassberger & Procaccia analysis should be validated by additional methods (Osborne & Provenzale 1989). One way to do this is to compute the largest Lyapunov exponent of the system. Lyapunov exponents are the average rates of divergence or convergence of nearby orbits in phase space. Since nearby orbits correspond to nearly identical states, exponential orbital divergence means that systems whose initial differences cannot be resolved will soon behave quite differently. Long-term predictions of chaotic systems are virtually impossible, even if the physics is known completely, because errors in measurement of the initial state propagate exponentially fast. A system is defined to be chaotic if it contains any positive Lyapunov exponent which is statistically significant. The magnitude of the largest positive exponent reflects the timescale on which the system becomes unpredictable.

Pulsar data are well suited for this type of analysis because some characteristics of the emission have an unpredictable and seemingly random nature. There are several reasons to pursue such an analysis. If the randomness can be identified with an underlying attractor of low dimension, this would imply that the dynamics can be described by a small number of parameters, comparable to the dimension of the space in which the attractor is embedded. Another use of this information is to test theoretical models. A theoretical model which displays a strange attractor of similar dimension with an attractor in the observational data would advance significantly the effort to solve the long-standing question of how pulsars operate.

There have been a number of studies which suggest that chaos is present in the time signals of pulsars, although none can be considered definitive. Romani, Rankin, & Backer (1992) examined pulse-to-pulse intensity records of PSRs B0823+26, B1929+10, and B1933+16. While two of the three pulsars showed behavior expected from random white noise, PSR B0823+26 seemed qualitatively different under the analysis of Grassberger & Procaccia. Romani et al. use this observation to infer that a dimension less than 2 applies to the radio signal from this pulsar, although an attractor is not established according to the techniques established by Grassberger & Procaccia. Zhuravlev & Popov (1990) examined the microstructure of 480 individual pulses from PSR B0809+74. In 20% of the pulses they find an attractor of dimension less than or equal to 5.3 using the Grassberger & Procaccia method. Because their data sets do not have the number of points required by theory to establish an attractor of this dimension, this attractor, too, may only be an artifact. Both the Romani et al. and the Zhuravlev & Popov analyses show that the behavior of some of the pulsar data sets is qualitatively different from white noise. However, to suggest that this behavior is due to an attractor is not rigorous, since purely stochastic data can also deviate from white noise.

A test of a specific emission theory requires a detailed description of the emitted pulse. A numerical model by one of us (Weatherall 1997, 1998) solves for the time evolution of the plasma wave turbulence in the pulsar source region. Conversion of this turbulence into electromagnetic emission is one of the proposed mechanisms for radio emission

[1] Present address: Department of Astronomy, University of Minnesota, Minneapolis, MN 55455.

(Asseo 1996). In this model, the emission derives from temporally transient and spatially localized wave structures in the turbulence and the superposition these individual "bursts" underlie the noise in the pulsar signal. If this process is generating the radio emission, the signal could be expected to share the statistics of the underlying turbulence. The numerical solutions for the turbulent generation of electromagnetic modes are detailed enough to apply the same time series analysis which is applied to the observational data. The results of this analysis are presented here. The computer solution for turbulent plasma emission shows that the bursts display deterministic behavior characterized by a strange attractor of dimension 2.09. Thus, this theory provides a clear prediction to test with observational data.

To test this idea, the time series analysis is applied to two pulsar data sets: an attractor is sought in both the nanostructure of the Crab pulsar (PSR B0531+21) and the timing and amplitude variations of the Vela pulsar (PSR B0833−45). Although the earlier studies of chaos in the time signals of pulsars provide some support for an attractor of finite dimension, there is no evidence for an attractor in the new data.

The analysis techniques, and how they apply to the Crab and Vela pulsar data, will be detailed next in § 2. The relationship of the plasma model data to the actual pulsar data is also described in § 2. Results of the analysis are presented in § 3. The discussion in § 4 addresses the limitations of the analysis relating to the present data and the qualifications attached to other chaos findings in pulsars. The success of the model in predicting chaos remains an open issue.

2. METHOD OF ANALYSIS

The correlation sum technique of Grassberger & Procaccia is the preferred method for computing dimension because it requires fewer data points than other methods and still gives a good result for the dimension because the scaling range for computing dimension is almost twice that of other methods (Greenside et al. 1982). Also, it is a very easy method to implement because it provides an estimate of dimension based purely on the statistics of pairwise distances. To apply this technique to time series data, the method of time delays (Packard et al. 1980; Takens 1981) is first used to reconstruct the phase space of the system. Given a measured time series of N points, $\{x(t_1), x(t_2), \ldots, x(t_N)\}$, the ith point on the trajectory in a phase space of n dimensions can be represented by using the vectors

$$\boldsymbol{X}(i) \equiv \{x(t_i), x(t_i + \tau), x(t_i + 2\tau), \ldots, x[t_i + (n-1)\tau]\} , \tag{1}$$

where n is the "embedding dimension" and τ is a fixed interval between observed points in the time series. For $n = 1$, the axis is $x(t)$. For $n = 2$, the "x-" axis is $x(t)$ and the "y-" axis is $x(t + \tau)$. For $n = 3$, the "x-" axis is $x(t)$, the "y-" axis is $x(t + \tau)$, and the "z-" axis is $x(t + 2\tau)$, and so on for higher dimensions. In this manner, the data set can be probed for the appropriate dimension of phase space needed to reconstruct the attractor.

Takens (1981) has provided a proof that this procedure does (almost always) reconstruct the original phase space of the system, as long as the embedding dimension $n > 2\nu + 1$, where ν is the dimension of the attractor. It should be noted, however, that as long as $n > \nu$, the reconstructed attractor will usually have the same dimension as the original attractor (Eckman & Ruelle 1985). The choice of delay time, τ, is almost arbitrary. If τ is too small (compared with the characteristic recurrence time of the system, which is the reciprocal of the dominant frequency obtained from the power spectrum), the trajectory is collapsed onto the diagonal in phase space because the points and their delays are almost equal. If τ is too large, then successive points are not well correlated and the trajectory is distorted. As long as τ lies between these two extremes, the reconstruction of the attractor and, hence, the measured dimension of that attractor, should not depend on the choice of τ. It is generally best, however, to choose the smallest possible delay time without causing diagonalization of the attractor (Buzug, Reimers, & Pfister 1990; Froehling et al. 1981).

The correlation sum is formally defined as

$$C(r) \equiv \lim_{N\to\infty} \frac{1}{N^2} \sum_{i=1}^{N} \sum_{j=1}^{N} \Theta[r - |\boldsymbol{X}(i) - \boldsymbol{X}(j)|] , \tag{2}$$

where Θ is the Heaviside function and $|\boldsymbol{X}|$ is the norm of the vector, $\boldsymbol{X}$. Although any norm will do, the Euclidean norm is used, which is defined in an n-dimensional space by

$$|\boldsymbol{X}(i) - \boldsymbol{X}(j)| \equiv \left\{ \sum_{k=1}^{n} [\boldsymbol{X}_k(i) - \boldsymbol{X}_k(j)]^2 \right\}^{1/2} , \tag{3}$$

where $\boldsymbol{X}_k$ is the kth element of the vector $\boldsymbol{X}$. For intervals r much smaller than the measure of the data set, $C(r)$ generally behaves as a power of r:

$$C(r) \propto r^m . \tag{4}$$

Evaluation of the correlation sum for several embedding dimensions gives a family of curves when plotted on log r versus log $C(r)$ axes. If the attractor is not fully embedded in a dimension or if there is no attractor, then the slope of the line, m, will be equal to the embedding dimension, n. If there is an attractor, and it is fully embedded, then the slope of the line, m, will be the dimension of the attractor, ν. The number of data points required to provide a good estimate of the dimension is $N \geq 10^{\nu/2}$ (Ruelle 1990); however, Abraham et al. (1986) make the argument that reliable dimension estimates can be made with smaller data sets.

Is it possible that this method could indicate an attractor, when in fact the system is purely stochastic? The answer to this question is yes; in particular, some systems with colored noise, namely noise which has a power-law spectrum with random, uniformly distributed Fourier phases, can give a false impression that the slopes are converging on an embedding dimension (Osborne & Provenzale 1989). The Harding, Shinbrot, & Cordes (1990) analysis of the Vela timing noise is an example where the method fails to discriminate between stochastic and chaotic signals. At the same time, all noise does not doom to failure the correlation sum method by affecting dimensions of nonexistent attractors or false dimensions of real attractors. For example, Theiler (1988) and Malraison et al. (1983) do not find attractors in systems which are dominated by noise. In other systems which do have real attractors, such as Shaw (1984) and Guckenheimer & Buznya (1983), the attractor still shows up in the correlation sum analysis, with the correct dimension, despite the existence of noise in the data.

The algorithm for computing dimension consists of choosing a point at random on the attractor and computing

the distance norm to all other points on the attractor. These distances are then sorted in order of distance to nearest neighbor, distance to next nearest neighbor, and so on. The process is repeated in a number of "trials" on other randomly selected data points on the attractor. The data from a series of trials are used to compute averages of these distances. When plotted on log L versus log N axes, where N is the number of points within a distance L, the correlation sum exponent, m, can be determined. We tested this method on the Lorenz, Rössler, & Hénon attractors and obtained dimensions of 2.05, 2.02, and 1.24, respectively. These numbers agree with published results (Grassberger & Procaccia 1983; Wolf et al. 1985).

Another measure of chaos is the Lyapunov exponent. It has the advantage that it is not fooled by the colored noises which give spurious results for the dimension algorithm. Its disadvantage is that accurate estimates of the Lyapunov exponents can only be derived from data sets with very good signal-to-noise ratios. Given a continuous dynamical system in an n-dimensional phase space, the long-term evolution of an infinitesimal n-sphere of initial conditions will produce an n-ellipsoid due to the locally deforming nature of the flow as the sphere moves along the trajectory. The ith one-dimensional Lyapunov exponent is then defined in terms of the length of the ellipsoidal principal axis $p_i(t)$:

$$\lambda_i = \lim_{t\to\infty} \frac{1}{t} \log_2 \frac{p_i(t)}{p_i(0)} . \quad (5)$$

The Lyapunov exponents are related to the expanding or contracting nature of different directions in phase space. If any Lyapunov exponent is positive, then chaotic motion is established. The exponents measure the rate at which system processes create or destroy information and are expressed in bits of information per time unit (Shaw 1981). If an attractor had an exponent of 2 bits per time unit, and an initial point were specified with an accuracy of one part per million (about 20 bits), then the future behavior of the system could not be predicted after about 10 time units [20 bits/(2 bits per time unit)].

A method developed by Wolf et al. (1985) is used to measure the largest Lyapunov exponent. It is known that an attractor reconstructed from the method of time delays has the same Lyapunov exponents as the original attractor. Therefore, to estimate the largest Lyapunov exponent (denoted by λ_1), Wolf's FORTRAN program recreates phase space by the method of time delays. By monitoring the distances between a single pair of nearby orbits along a fiducial trajectory through the entire data file, λ_1 is estimated. We tested the algorithm on the Rössler attractor with a result of 0.112 for the largest Lyapunov exponent (Wolf gets 0.13). The test was also applied to a limit cycle, $\lambda_1 = 0$, and a decaying orbit, $\lambda_1 = -0.18$, which are sensible results. This Lyapunov exponent test is useful because it can provide an independent confirmation of positive results from the dimensional analysis. However, because this analysis relies on very clean data sets for accuracy, it is only applied to the pulsar model data.

The methods outlined above have been successful in documenting chaos in laboratory systems when a probe is placed at a fixed point in the fluid to measure something about the flow, such as direction or speed, as a function of time (Gollub & Swinney 1975). What is it that is being measured by the remote detection of pulsar radio emission? In the context of the plasma turbulence model, the radio emission from an individual burst is a measure of the local electric field in a single coherent wave structure: thus, radio emission serves exactly like a probe in the laboratory experiment. Unfortunately, this idealization of a single, resolved burst is only realized in the computer model.

The Crab pulsar data sets sample the emission on very short timescales, but not short enough to resolve an individual burst. We infer that these data sample a localized volume (the light transit distance is very small over 10 ns) involving either a collection of bursting wave structures or a repeating bursting structure. Here the temporal modulation of the radio emission could be a measure of burst rate or burst intensity. The amount of rotational phase that occurs during a giant pulse is very small.

In the Vela pulsar data sets, the radio emission becomes a measure of the rotational phase of the region in the magnetosphere which has the greatest emissivity due to turbulent activity. The phase of an individual pulse appears to be positioned randomly within the average emission profile. Assuming that the height of the emission above the polar cap is constant, which is consistent with radius-to-frequency mapping (Thorsett 1991; Komesaroff, Morris, & Cooke 1970), the phase corresponds to a spatial position in the plasma magnetosphere. Thus, during each rotational cycle, the turbulent emission maps to a different location in the magnetospheric emission region.

Of course, the prediction of chaos by one standard of measure (burst electric field) does not necessarily carry over to other measures (burst rate or burst position). Also, bursty turbulence provides a conceptual meaning to the emission measurement but does not need to be correct in order for the test of observational data to be valid. Our search for an attractor relies only on the assumption that the signal contains information about the behavior of the emission source.

2.1. *Application to Crab Pulsar Data*

Observations of single giant pulses of the Crab pulsar were used for this analysis (Moffett 1997). The data include VLA[2] observations at L band (1435.1 MHz), C band (4885.1 MHz), and X band (8414.1 MHz) and at a time resolution of 10 ns and a bandwidth of 50 MHz. The right- and left-circular polarizations were sampled directly, and the dedispersion techniques of Hankins & Rickett (1975) were used to reconstruct the pulse. The circular polarizations were then summed to form the total intensity. In Figure 1 the intensity curve for an X-band giant pulse is shown along with the corresponding right- and left-hand circular polarizations.

The data analyzed consisted of the following records:

1. Thirty-eight total intensity records in the three bands. The number of data points ranged from 200 to 5000 per pulse.

2. Forty records of right- and left-circular polarization predetection voltages, with the same range of data points.

The interval for the time series is $\tau = 10$ ns, which is the time between each data point; since nearby data points do not have nearly the same value (because they are Nyquist samples of the 50 MHz bandwidth), there is no danger of

[2] The VLA is a telescope of the National Radio Astronomy Observatory, which is operated by Associated Universities, Inc., under a cooperative agreement with the National Science Foundation.

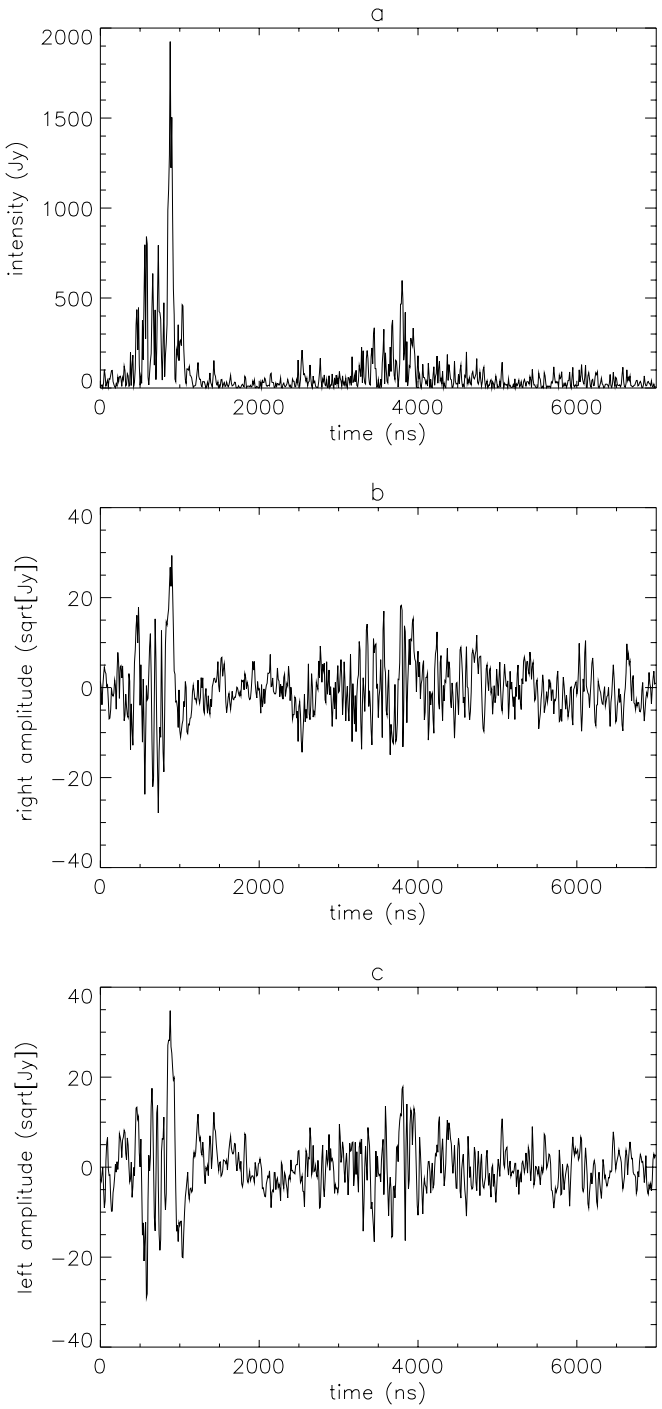

FIG. 1.—Giant pulse of the Crab pulsar at X band with 10 ns resolution and a bandwidth of 50 MHz. (*a*) Total intensity; (*b*) intensity of right-hand circular polarization; and (*c*) intensity of left-hand circular polarization.

diagonalizing the attractor (assuming one is present). A large number of trials was used to attain power-law behavior for the correlation function. For the smaller data sets, 75% of the points were selected at random as the initial test point for individual trials. For good results from the larger data sets, 40% of the data points were used as trials.

2.2. *Application to Vela Pulsar Data*

The Vela pulsar data were acquired with the VLA by using the 28 detected output channels of the Mark 3 video converter to sample the 28 individual channels from the Mark 3 video detector. Each channel had a 1 MHz bandwidth with a 200 μs time constant and a sampling rate of 10.08 kHz. These data were taken at L band (1435.1 MHz). The pulse amplitude and timing were measured for each period based on the point on each pulse with the largest magnitude. In cases where there were several points with the largest magnitude (sawtooth or flat top), time was measured at the first point. Because the position of these amplitude and timing points is affected by the system noise, the integrated flux of each pulse was measured as well as the times of arrival of the *centroid* of each pulse.

Four different aspects of this data set were analyzed:

1. Pulse peak intensity for three frequency channels in a 7 minute data record and for two frequency channels in a second 7 minute data record. The data sets have approximately 4700 points.
2. Pulse-to-pulse interval, measured between the peaks of the pulses, for the same data.
3. The integrated flux of each pulse for this data set.
4. Pulse-to-pulse interval, measured between the centroids of the pulses for the same data.

The pulse-to-pulse intervals measure the arrival time fluctuations with respect to the underlying period. The signal amplitude variation and arrival time fluctuations would appear to be connected to activity in the pulsar magnetosphere.

Although the data are sampled at regular intervals (or almost regular intervals, considering the way the resulting data sets are constructed), the system is not being continuously sampled because we only have access to the system when the signal sweeps across our field of view. Because our access to the system is roughly periodic, a plot of one pulse interval (or amplitude, or flux) versus the next pulse interval (or amplitude, or flux) recreates a Poincaré cross section of the phase-space trajectory, rather than the phase-space trajectory itself. A dimensional analysis can be performed on the data as before, but the cross section will have a dimension one less than the dimension of an actual attractor. (This is similar to the water drop analysis described by Shaw 1984.)

Note that instead of adding all 28 frequency channels together, the test was conducted on a single frequency channel of data at a time. There was some variation due to pulses lost in the noise, pulses lost in the VLA waveguide switch cycle, and a few spurious noise spikes. The delay time for the time series was equal to 1 for the same reason as the Crab pulsar data. The number of trials for each data set was selected from 50% to 60% of the total data. Figure 2 shows the first seven pulses of the first data set. Also pictured are plots of the first hundred pulse peaks and pulse intervals.

2.3. *Application to Pulsar Model*

The theoretical description of the pulsar radio emission is inferred from a model of nonlinear wave processes in the pulsar magnetosphere. The turbulence model consists of modal equations coupled through a cubic nonlinearity (Weatherall 1997). Although the wavemodes are specific to the strongly magnetized pair plasma, the governing equation resembles the nonlinear Schrödinger equation, which is known to have a strange attractor (Russell & Ott 1981; Wersinger et al. 1980a, 1980b).

According to this model, a two-stream instability in the polar cap flow builds up amplitude in an electrostatic mode.

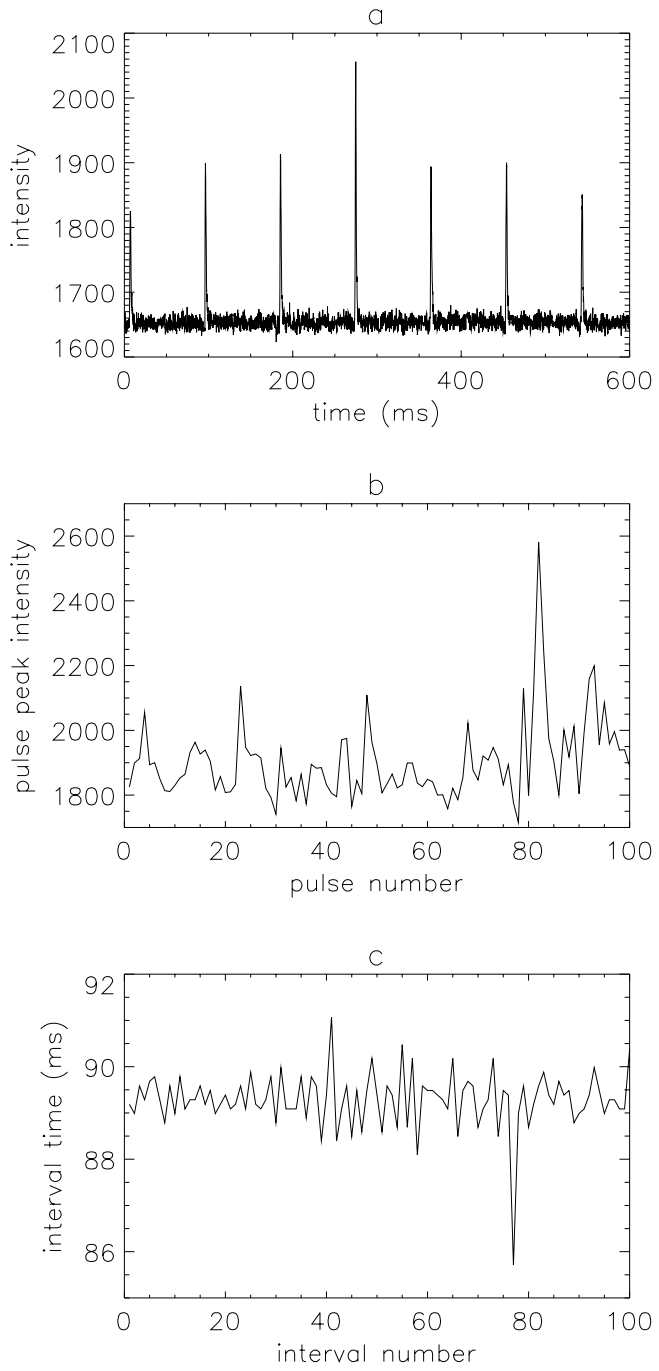

FIG. 2.—Vela pulsar data from a 1 MHz wide channel at L band with sampling rate of 10.08 kHz. (*a*) Total intensity in the first seven pulses (the intensity is in computer sampling units and is not calibrated to zero); (*b*) the peak intensities of the first hundred pulses (the integrated flux is similar); (*c*) pulse-to-pulse intervals for the first hundred pulses (the pulse centroids are similar).

As this mode reaches large amplitude, subsequent wave-wave interactions, identified with oscillating two-stream and modulational instabilities, transport energy into other wavemodes. The stimulated waves have dispersion characteristics of the fast branch of the ordinary mode, which means that they are electromagnetic and superluminal and can escape the plasma as radiation. Further nonlinear interaction produces filamentation of the initial beam-resonant wave, formation of soliton-like wave structures, and the "collapse" of the wave energy into spatially localized regions. These phenomena are all characteristic of strong plasma turbulence (Zakharov 1972; Goldman 1984). The numerical solutions also reveal a recurrent behavior, in which part of the system energy resonates back and forth between the nonlinear state and the initial state (Yuen & Ferguson 1978; Thyagaraja 1979). Recurrence is a property associated with chaotic systems.

The numerical model shows pulsar radio emission as a nonlinear transition to strong plasma turbulence following the slow buildup of electrostatic energy in plasma waves. Because the turbulence is nonsteady, the radio emission is intermittent.

The output of the pulsar turbulence code is the amplitude of one of the wavemodes generated in the turbulence. This mode is characteristic of the modulationally excited mode and is singled out because it is the largest amplitude of all the secondary electromagnetic modes. The data include very detailed information about the waveform during a single cycle of growth, saturation, and depletion by radiative loss. This information details the "nanostructure" of an individual "burst." Longer computer runs follow many cycles and provide strings of these bursts. The time between bursts is governed by an evolutionary timescale associated with the growth cycle of the turbulence and is much less than the rotational period of the pulsar. There could be several hundred bursts in a single Crab pulsar giant pulse.

The chaos analysis is applied to the following:

1. A computer-generated nanostructure data set, following the time history of the amplitude of one of the modulationally generated modes during a single nonlinear burst cycle, with a resolution of 7817 points.
2. Two data sets derived from an extended computer generated solution of the modulationally generated mode. The solution followed the continuous development of 650 nonlinear bursts. One data set consists of the series of burst timing; the second data set consists of the sequence of burst intensity.

Although it is known that the phase space of the numerical model consists of the amplitudes of 64×64 modes, the method of time delays is used to reconstruct the phase space for the model, anticipating that it has less than 4096 axes.

Figure 3 shows the electric field amplitude versus time for the nanostructure solution. The in situ amplitude is derived from assumptions of temperature and density in the Crab

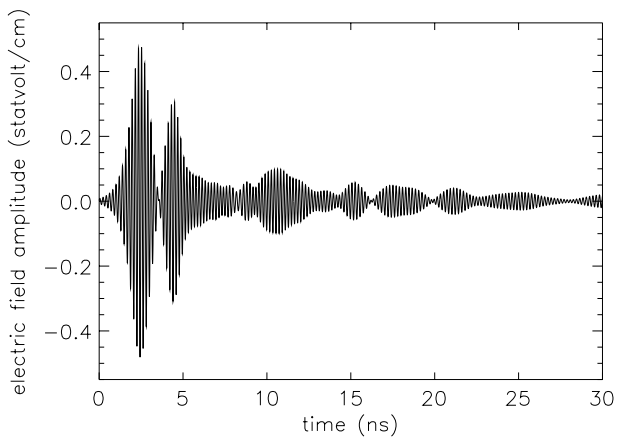

FIG. 3.—Nanostructure in a simulated burst. The timescale and electric field amplitude are derived assuming a plasma frequency of 5 GHz for a pulsar similar to the Crab pulsar.

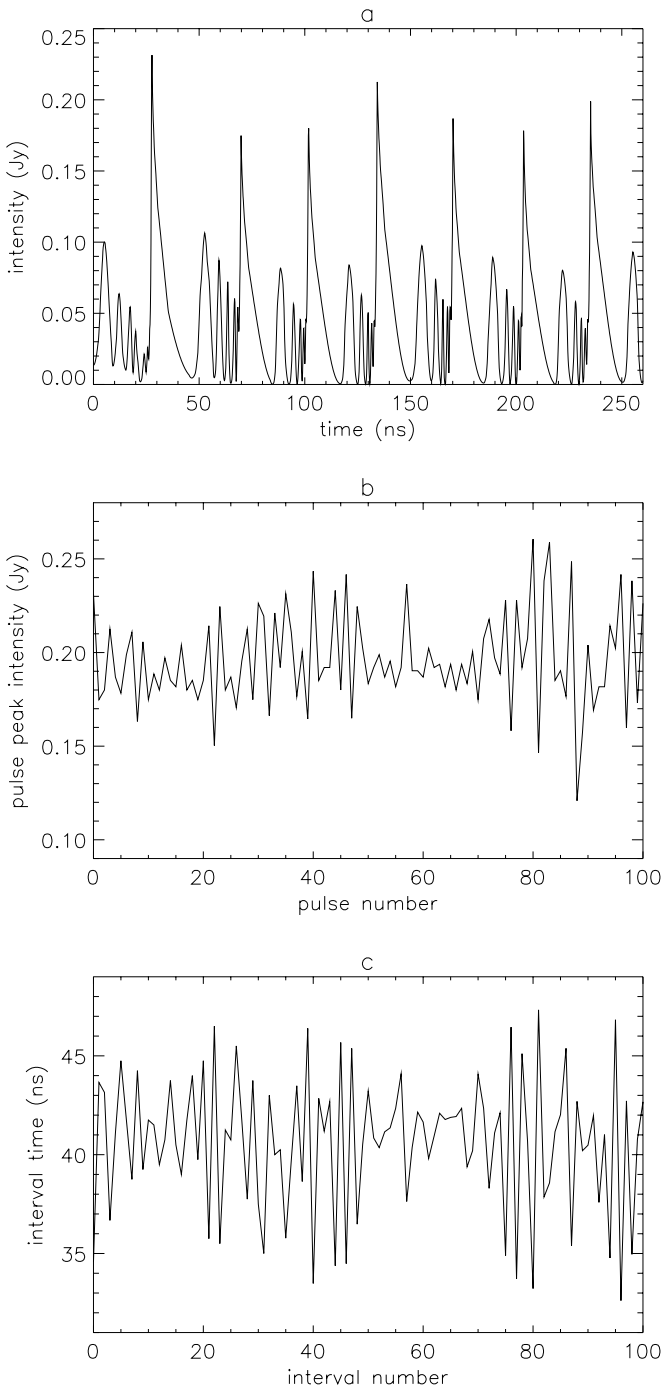

FIG. 4.—Computer model emission data. (*a*) A string of seven bursts simulating an amplitude-squared detection at 5 GHz and assuming Crab pulsar characteristics; (*b*) the peak intensities of the first 100 bursts; and (*c*) burst-to-burst intervals for the first 100 bursts.

pulsar magnetosphere (Weatherall 1997). At an observational frequency of 5 GHz, the timescale for the whole burst is approximately 15 ns. The modulational structure on the scale of 2 ns derives from the recurrent behavior described above. The burst shown here was tested with the delay time, τ, equal to 1, and with 2000 trials.

To analyze the burst string, the computer data were used to simulate an amplitude-squared detection by a radio telescope. The procedure for identifying the burst peaks and measuring the burst intervals is the same as used for the Vela pulse data. Figure 4 shows the first seven bursts of the simulation along with plots of the first hundred burst peaks and burst intervals. The timescale between bursts is approximately 40 ns. The intensity derives from model-dependent assumptions (Weatherall 1997). Note, in comparison, that the typical pulsed radio intensity from the Crab pulsar at C band is slightly above 0.5 mJy, although giant peaks are detected up to 1000 Jy (Moffett & Hankins 1996). The data were processed the same as the Vela pulsar data, with delay interval equal to 1 and the number of trials at 90% of the total data points.

3. RESULTS

3.1. *Crab Pulsar*

Figure 5*a* shows a typical correlation sum plot, log L versus log N, for the Crab nanopulse data. This particular plot is for the right-circular polarization in Figure 1. At small N and L there are too few points to make an accurate slope measurement. At large N and L there is a turnover due to the finite size of the data set: since all of the points are already included in the sum, the correlation sum satu-

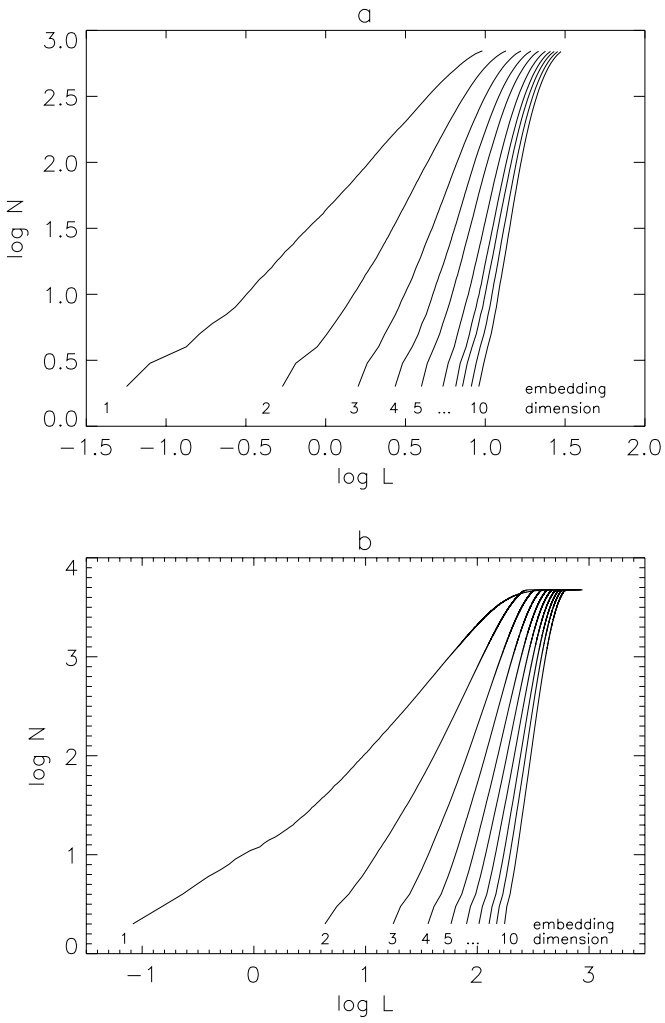

FIG. 5.—(*a*) Correlation sum for the right-hand circular polarization intensity of Fig. 1 (the Crab pulsar). The curves are for embedding dimensions 1–10. If an attractor were present, the slopes of the curves would converge to the value of the dimension of the attractor. Because the slopes of the lines do not converge, there is no evidence for a chaotic attractor. (*b*) The correlation sum for the pulse peak intensity data of Fig. 4 (the Vela pulsar).

rates. The appropriate scaling region for computing slopes is between these two extremes. Since the slopes of the lines are essentially equal to the embedding dimensions, there is no evidence for a chaotic attractor of low dimension. This particular plot involved 700 data points and 650 trials. The analysis is accurate up to dimension 5.7. The correlation sum was done for higher embedding dimensions in case the attractor required higher embedding to be seen. This analysis does not preclude the presence of an attractor in the data, only the presence of an attractor of dimension less than 5.7. There is no evidence in any of the intensity and polarization records to indicate the presence of deterministic chaos.

3.2. *Vela Pulsar*

The Vela pulse-to-pulse peak, peak interval, integrated flux, and pulse centroid interval data show no indications of a low-dimensional chaotic attractor, either. Figure 5*b* shows a typical correlation sum plot for the intensity, flux, and both interval analyses. The data set for this plot consisted of 4755 peak data points with 3000 trials. The analysis is good to dimension 7.4.

To evaluate the possibility that noise is responsible for the null results, the effect of noise on the Rössler attractor was explored. Details of this analysis are included in the Appendix. It is found that the correlation sum of Grassberger & Procaccia can tolerate signal-to-noise ratios of about 30–40 and still reveal evidence for an attractor. The signal-to-noise ratios for our data range from a few tens to about 100 for the Crab pulsar giant pulses and to about 100 for the Vela Pulsar flux and centroid interval data (T. H. Hankins 1997, private communication). Over half of the data sets tested were over the noise limit set by the Rössler test, excluding noise as a factor in those cases.

3.3. *Pulsar Model*

The correlation sum for the simulated burst nanostructure in Figure 3 is shown in Figure 6*a*, along with the corresponding attractor in Figure 6*b*. For the case of the model data, the slopes of the lines converge to the dimension of the attractor by embedding dimension 3. By embedding dimension 7, the attractor is fully embedded and the slope is constant over a larger range than previous embedding dimensions. The area between the dashed lines denotes the scaling region. The correlation curve above the top line is disregarded because the finite length of the data set affects the time delay analysis, as described in § 3.1 and also because of the elbow in the curve above that point. Elbows such as this are typically disregarded in dimensional analysis (see, for instance, Grassberger & Procaccia 1983). The curve below the bottom line is affected by poor statistics on the smallest scales. Least-squares fitting to a line in the range of the scaling region gives the slopes of lines 5–10. The average of these six slopes gives a value of 2.09, with a scatter of ± 0.05.

This result can be compared with Russell & Ott (1981) who find a dimension of 2.3 for a basic form of the nonlinear Schrödinger equation. Because the pulsar model involves a nonlinear Schrödinger-like equation, a comparable attractor might be expected. However, the pulsar model includes substantial damping in some of the modes (this is due to radiative loss), as well as modified dispersion and coupling characteristics due to the wavemodes specific to the magnetized pair plasma. Given these differences, the value for the

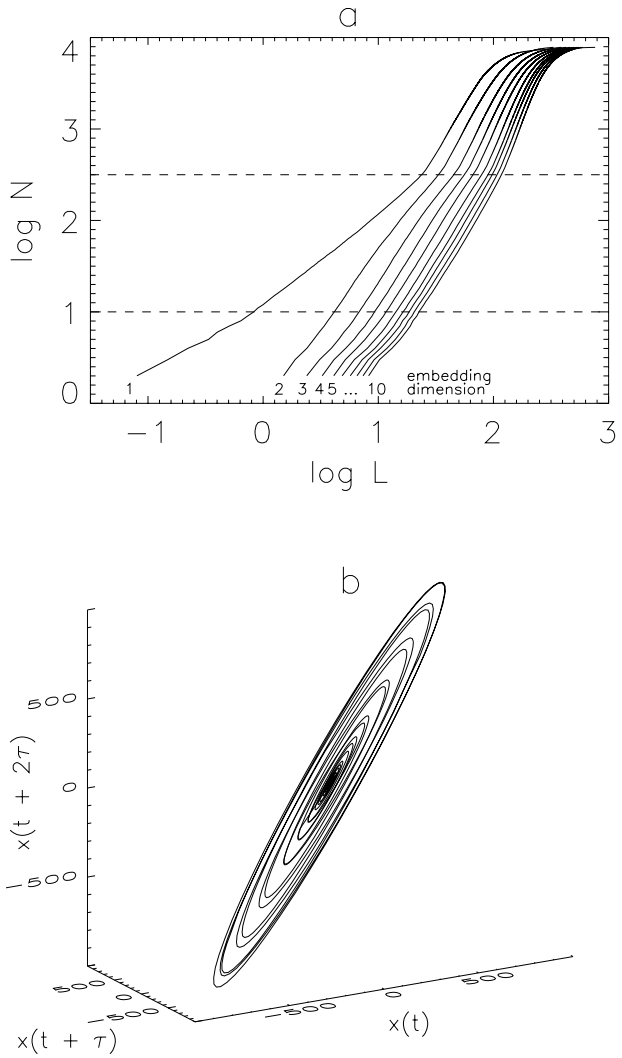

FIG. 6.—(*a*) Correlation sum for the pulsar model burst in Fig. 3 (nanostructure data). The area between the dashed lines was chosen as the scaling region. Because the slopes of the lines converge to a value of 2.09 by dimension 3, this is evidence for a chaotic attractor. (*b*) The corresponding phase-space plot for the attractor in the nanostructure data reconstructed from successive values of the electric field amplitude. These values have not been scaled to the values in Fig. 3.

attractor dimension should not be expected to be exactly the same. Note also that Russell & Ott analyzed the actual attractor, not the reconstructed attractor as shown here.

Although the dimension of the attractor is found to be close to 2, it is not *exactly* 2 because the trajectory shown in Figure 6*b* is manifestly not a limit torus. This is important because an attractor of integer dimension is a simple attractor and such a system does not display chaotic behavior. The calculation of the Lyapunov exponent described next will further establish that the system is chaotic. Finally, the fact that trajectories cross in two-dimensional space can be consistent with solution uniqueness only when the dimension is greater than 2.

Steep power spectra are often found in data with colored noise and can fool the Grassberger & Procaccia test into revealing small dimensional attractors when none are present (Osborne & Provenzale 1989). Because the pulsar model nanostructure data have a fairly steep power spec-

TABLE 1

INPUT PARAMETERS FOR WOLF ET AL. LYAPUNOV CODE

Symbol	Description	Value
npt	Number of data points	7817
dim	Embedding dimension	3–7
tau	Reconstruction time delay	8
dt	Time between each data point	0.13
scalmx	Upper limit to scaling region	5–14
scalmn	Lower limit to scaling region	1–7
evolv	Time to follow divergence of two initial points	25–50

trum (Weatherall 1998), it is helpful to confirm the chaos finding by deriving the Lyapunov exponent. For this purpose, the FORTRAN program of Wolf et al. (1985) is used, with the input parameters given in Table 1. The time units in the code are scaled to the local plasma frequency, where one time unit corresponds to 0.03 ns in Figure 3. The largest Lyapunov exponent is computed to be 0.11 ± 0.02 bits per time unit. This nonzero, positive exponent confirms the presence of chaos in the pulsar model nanopulse.

The behavior of the numerical solutions is also consistent with an exponential divergence of nearly identical initial conditions. This was manifest in comparison of solutions with different time steps. According to the Lyapunov exponent, if the precision in the solution is one part per million, the behavior is predictable for time $T \sim 200$ time units. Decreasing the time increment always improved the measure of energy conservation, as expected with a second-order accurate (double precision) algorithm. However, the consistency in the burst detail was lost after about 40 oscillations.

Despite the success with the nanostructure model data, the burst-to-burst variation in the longer timescale string of bursts does not show an attractor. Figure 7 shows the correlation sum plot for the burst interval analysis. The burst amplitude analysis is very similar.

4. DISCUSSION

The lack of a correlation dimension in the Crab and Vela pulsar data does not necessarily mean that there is no attractor. It merely means that there is no attractor of low dimension. If there were a low-dimensional attractor, it is unlikely that noise alone could be responsible for masking it, as discussed in the Appendix. Although the noise analysis was conducted on a 2500 point data set, over half of our pulsar data sets were over 2500 points. Therefore, if noise were the culprit in the small data sets (fewer than 2500 points), the attractor would still be apparent in the larger data sets; but this is not the case. Another possibility is that the actual phase space of the system does not include intensity, integrated flux, pulse interval, or polarization. If the chosen coordinates are not state variables of the system, they will not recreate an attractor even if the system is chaotic.

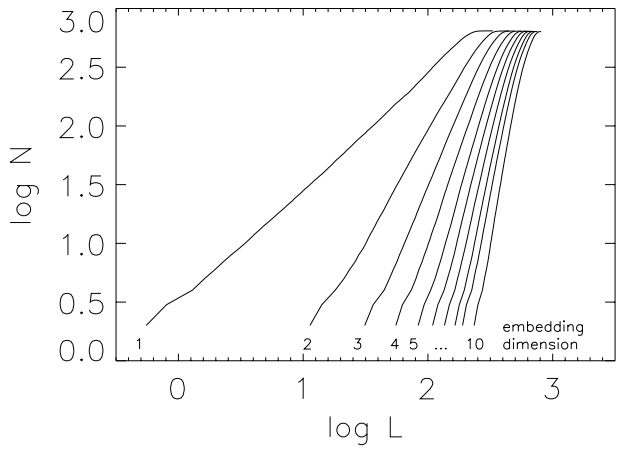

FIG. 7.—Correlation sum for the pulsar model burst intervals in Fig. 4. Because the slopes of the lines do not converge, there is no evidence for a chaotic attractor.

A concern with the analysis of pulsar data is the effect of scattering media on the signal. The two pulsars being studied are also associated with supernova remnants, which enhance the scattering. If the scattering is large enough, all traces of an attractor could be lost: the photons would not be reaching us in the same order they were emitted, and, consequently, the method of time delays would not accurately reconstruct the phase space of the system. At X band, the scattering timescale is less than the sampling interval, however, at C and L band, the scattering timescale is large enough to affect photon order. A concern regarding the Vela pulsar data is whether the radio emission is a useful probe of plasma turbulence over different rotation periods. Finally, the way in which points for the pulse-to-pulse variations in the Vela pulsar data were chosen could introduce some scatter into the ideal data set (whatever that might be), although this scatter would seem to be less important than the noise (Shaw 1984).

The correlation dimension of 2.09 for the pulsar model nanostructure means that, although the model consists of thousands of modes, something on the order of three state variables are responsible for the emission process. This suggests that a derivative model like Main & Benford (1989), which is based on rate equations for the amplitudes of a small set of modes, may describe many essential features of the turbulence and the emission.

Since the computer model shows chaos on the timescale of the bursts, it is interesting that the attractor disappears on the burst-to-burst timescale. In accounting for the fact that the burst-to-burst variations of the model do not reveal an attractor, several possibilities must be allowed. First, the system may actually be chaotic only on short timescales. Second, an attractor in these variations may be of higher dimension than could be calculated from the data. Third, the scatter introduced in constructing the Poincaré cross section from burst peaks and burst intervals may be a more important deviation than implied by Shaw. Finally, if an attractor on the larger timescales does exist, it may not include the variables chosen for the analysis.

The pulsar data fail to display the attractor predicted by the computer model. This is not a decisive rejection of the turbulent emission mechanism because there are many qualifications. On timescales of 40 ns, the model agrees with the data in that neither show chaotic behavior (the burst-to-burst analysis is valid for timescales ≥ 40 ns, and the Crab nanostructure is valid for timescales ≥ 10 ns). Furthermore, the computer model for emission is limited to the effect of single bursts. The actual phenomenology of pulsar emission, if it involves a superposition of bursts emitted at different time and from different locations, may obscure any attractors underlying individual bursts. For a definitive analysis, pulsar data need to be tested on shorter timescales

TABLE 2

STUDIES OF CHAOS IN PULSAR SIGNALS

Pulsar	P (s)	$P/\dot{P}$ (yr)	Type[a]	DM (pc cm^{-3})	f (GHz)	Δf (MHz)	Δt (s)	τ (s)	N	ν
B0833−45[b]	0.089	2×10^4	D	68.2	2.4	12	25×10^{-6}	$4 \times 10^{+6}$	564[b]	1.5
B0809+74[c]	1.292	2×10^8	T	5.8	0.1	?[d]	10×10^{-6}	10×10^{-6}	512/1024[c]	$\lesssim 5$
B0823+26[e]	0.531	1×10^7	S_t	19.5	1.4	10	0.4×10^{-3}	0.531	6200[e]	$\lesssim 2$
B1929+10[e]	0.227	6×10^6	T	3.2	1.4	10	0.2×10^{-3}	0.227	3472[e]	...
B1933+16[e]	0.359	2×10^6	T	158.5	1.4	1	0.2×10^{-3}	0.359	2403[e]	...
B0833−45[f]	0.089	2×10^4	D	68.2	1.4	1	0.1×10^{-3}	≈ 0.089	4700[f]	...
B0531+21[g]	0.033	3×10^3	Mix[h]	56.8	1.4	50	10×10^{-9}	10×10^{-9}	200–5000[g]	...
B0531+21[g]	0.033	3×10^3	Mix[h]	56.8	4.9	50	10×10^{-9}	10×10^{-9}	200–5000[g]	...
B0531+21[g]	0.033	3×10^3	Mix[h]	56.8	8.4	50	10×10^{-9}	10×10^{-9}	200–5000[g]	...
Model[i]	...	...	...	...	5.0	∞	0.4×10^{-9}	$\approx 40 \times 10^{-9}$	650[i]	...
Model[j]	...	...	...	...	5.0	∞	0.03×10^{-9}	0.03×10^{-9}	7817[j]	2.09

NOTE.—Symbols: P = period; $\dot{P}$ = period derivative; DM = dispersion measure; f = observation frequency; Δf = bandwidth; Δt = timing resolution; τ = delay time; N = number of points in data sets; ν = dimension of attractor found.

[a] Rankin 1983.

[b] Harding et al. 1990: long-term timing residuals.

[c] Zhuravlev & Popov 1990: single pulse intensity microstructure.

[d] Zhuravlev & Popov did not report the bandwidth for their observations.

[e] Romani et al. 1992: pulse-to-pulse intensity.

[f] This paper: Vela pulsar pulse intensity (peak) and integrated flux and pulse-to-pulse interval.

[g] This paper: single pulse intensity nanostructure of Crab giant pulse.

[h] Not classified: the morphology of the Crab pulsar profile is not understood.

[i] This paper: burst intensity (peak) and burst-to-burst interval.

[j] This paper: single burst intensity.

in the hope of resolving individual bursts. Also, to eliminate (or lessen) the problem of scattering, pulsars in which scattering is known to be weak should be studied.

The claims that attractors have been found in other pulsar data sets should be examined critically. Some differences in the data sets which might contribute to different outcomes include time resolution, number of data points, pulsar period and age, dispersion measure, and core/cone pulse profile characteristics (Rankin 1983); these are summarized in Table 2. However, our interpretation of the evidence presented in the published analyses would not lead us to conclude that the pulsar radio emission is deterministic. Romani et al. (1992) find that the correlation sum slopes derived from the pulse-to-pulse intensity records of PSR B0823+26 differ from those of random white noise around dimension 2. However suggestive, this departure from white noise does not establish the existence of an attractor (Grassberger 1987). Zhuravlev & Popov (1990) find an attractor of dimension less than or equal to 5.3 in the microstructure intensity of PSR B0809+74. This number is much higher than predicted by the model, although they were probing structure on 10 μs scales rather than 0.03 ns scales. However, their data sets are fairly small—512 points in most of their tests, 1024 in a few cases. This limits them to only searching for a dimension of less than 5.42 (6.02 for the larger sets). It is possible for the correlation sum to saturate to the limiting dimension at large embeddings even if no attractor is present (Ruelle 1990). Because their correlation sum does not converge until around embedding dimension 20, their results may suffer from this phenomenon. Another study done by Harding et al. (1990) examined 14 yr of phase residuals from the Vela pulsar; using the Grassberger & Procaccia technique, they find an attractor of dimension 1.5. The authors suggest that these results could be confusing chaos with steep power spectrum noise. There is no useful comparison to either the model or the data in this work anyway, because it probes structure on very long timescales. We conclude that there is no evidence of low-dimensional attractors in pulsar radio data.

The search for attractors in pulsar radio signals needs to be pursued with data of higher time resolution in order to make a better comparison with theory. Not only should the data sets be longer and of higher quality, but they should include different measures about the pulsar than just intensity and pulse arrival time. These measures could include pulse-to-pulse variations of percent linear (or circular) polarization and pulse widths. For individual pulse microstructure and nanostructure, the Stokes parameters Q, U, and V could also be tested for evidence of deterministic chaos. Furthermore, several independent tests for chaos must be applied to the data to avoid false positive results. Currently, any low-dimensional attractor found in the nanostructure signal can be compared with an attractor of dimension slightly above 2 predicted by the pulsar turbulent emission model. More theoretical models should be tested to provide a larger base for comparison with actual pulsars. Unfortunately, chaos theory has not yet helped in the quest to further understand the pulsar emission process.

This work has been conducted with partial support by NSF grants AST 96-18408 and AST 93-15285. We thank Tim Hankins and Dave Moffett for providing data for the analysis and also Jean Eilek and Paul Arendt for valuable conversations.

APPENDIX A

THE EFFECT OF NOISE ON AN ATTRACTOR

The Rössler attractor is used to evaluate the effect of noise on the utility of the Grassberger & Procaccia correlation sum method to identify an attractor. The Rössler data derive from the differential equations,

$$\frac{dx}{dt} = -(y + z) ,$$

$$\frac{dy}{dt} = x + 0.15y , \tag{A1}$$

$$\frac{dz}{dt} = 0.2 + xz - 10z ,$$

for the x-variable. The method of delays is used to reconstruct the attractor, and the dimension is computed from the correlation sum analysis. The analysis is repeated after adding a Gaussian noise term to each x-value. Signal to noise ratios (S/Ns) range from infinity (no noise) to 0.5, with the S/N computed from the variance of the signal divided by the variance of the noise. To get an accurate indication of the effects of noise on the pulsar data, data sets of similar size (2500 points) were generated, and trials of similar number (1000 trials) were used.

Figure 8 is the reconstructed attractor with no noise, Figure 9 shows the first 200 data points for a range of S/Ns, and Figure 10 is the dimensional analysis for each of those S/Ns. The slopes for the attractor alone clearly converge to the dimension of the attractor by dimension 3. By decreasing the S/N, the slope scaling region decreases. At low N and L the slope begins to equal the embedding dimension. As the ratio is decreased even further, the values of N and L where the slope deviates from the dimension increase. Another effect of the noise is to slightly increase the value of the slopes in the scaling region, although they are nowhere near the value of the embedding dimension. Similarly, the embedding dimension where the slope starts to converge on the dimension of the attractor increases. Even though attractor remnants can be seen in the very low S/N plot, without comparison with the other plots in the series, the analysis by itself would not be clear evidence for a chaotic attractor. In summary, the correlation sum of Grassberger & Procaccia can tolerate S/Ns of about 30–40 and still reveal evidence for an attractor, although the dimension will be overestimated.

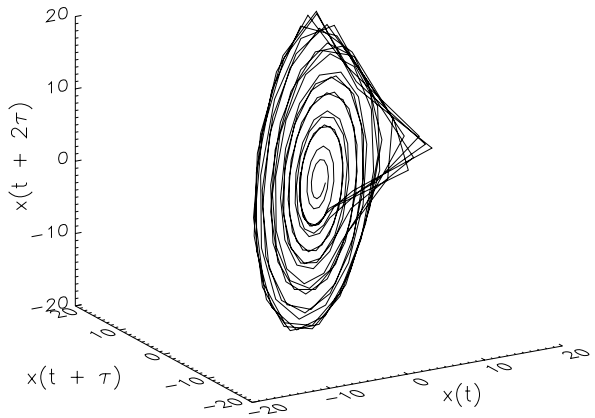

FIG. 8.—Reconstruction of the Rössler attractor from the x-variable of the solved differential equations using the method of time delays. This reconstruction is for an ideal data set with no noise.

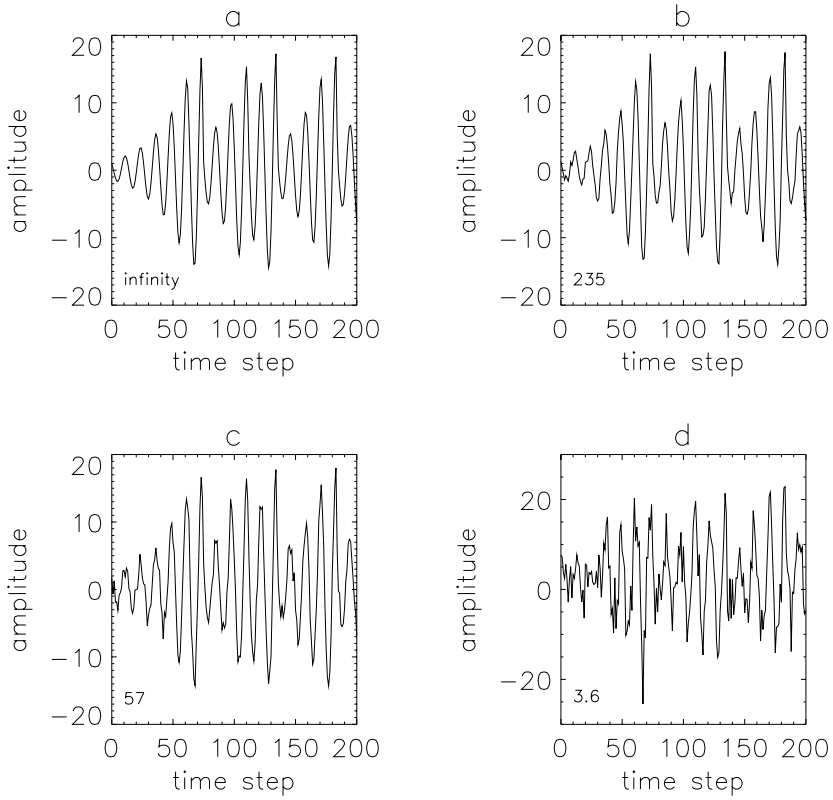

FIG. 9.—First 200 x-values for the Rössler attractor with a Gaussian noise term added to each value. The approximate signal-to-noise ratio is indicated in the lower left-hand corner of each plot. The correlation sums for this analysis are in Fig. 10.

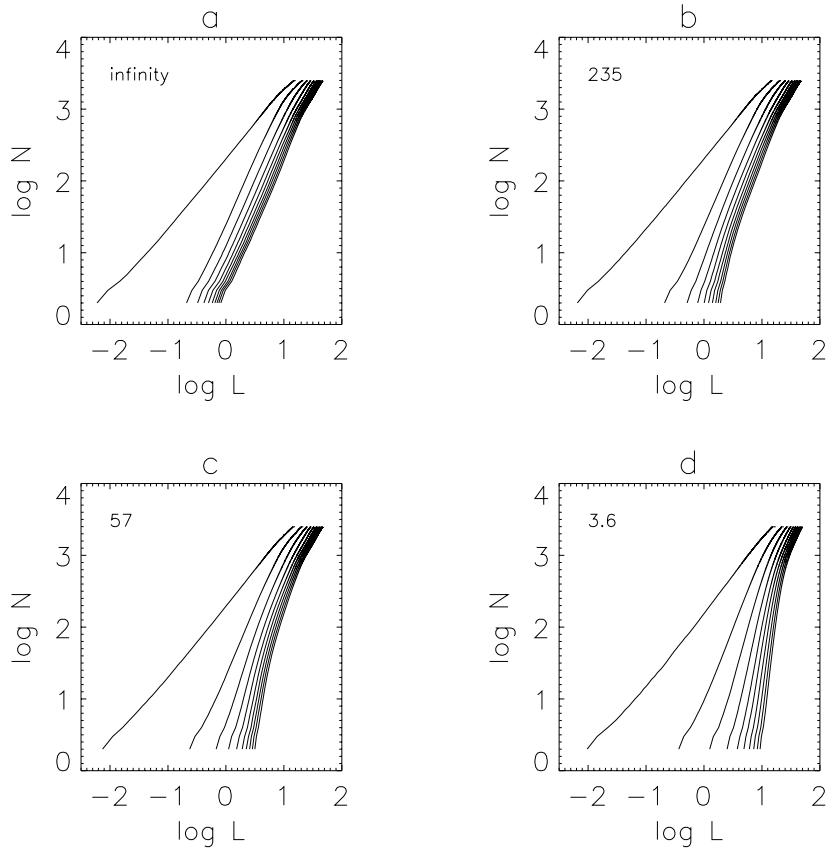

FIG. 10.—Correlation sums for the Rössler attractor noise analysis of Fig. 9. As noise is added, the scaling region for taking slopes decreases and the slopes in the scaling regions increase until all evidence of the underlying attractor disappears. The approximate signal-to-noise ratio is indicated in the upper left-hand corner of each plot.

REFERENCES

Abraham, N. B., et al. 1986, Phys. Lett. A, 114, 217
Asseo, E. 1996, in Pulsars: Problems and Progress, IAU Colloq. 160, ed. S. Johnston, M. A. Walker, & M. Bailes (San Francisco: ASP), 147
Buzug, Th., Reimers, T., & Pfister, G. 1990, Europhys. Lett., 13, 605
Eckman, J.-P., & Ruelle, D. 1985, Rev. Mod. Phys., 57, 617
Froehling, H., et al. 1981, Physica D, 3, 605
Goldman, M. V. 1984, Rev. Mod. Phys., 56, 709
Gollub, J. P., & Swinney, H. L. 1975, Phys. Rev. Lett., 35, 927
Grassberger, P. 1987, Nature, 326, 524
Grassberger, P., & Procaccia, I. 1983, Phys. Rev. Lett., 50, 346
Greenside, H. S., et al. 1982, Phys. Rev. A, 25, 3453
Guckenheimer, J., & Buznya, G. 1983, Phys. Rev. Lett., 51, 1438
Hankins, T. H., & Rickett, B. J. 1975, in Methods in Computational Physics: Advances in Research and Applications, Vol. 14: Radio Astronomy, ed. B. Alder et al. (New York: Academic), 55
Harding, A. K., Shinbrot, T., & Cordes, J. M. 1990, ApJ, 353, 588
Komesaroff, M. M., Morris, D., & Cooke, D. J. 1970, ApJ, 5, L37
Main, W., & Benford, G. 1989, Phys. Fluids B, 1, 2479
Malraison, B., et al. 1983, J. Phys., Lett., 44, L897
Moffett, D. A. 1997, Ph.D. thesis, New Mexico Inst. Mining Tech.
Moffett, D. A., & Hankins, T. H. 1996, ApJ, 468, 779
Osborne, A. R., & Provenzale, A. 1989, Physica D, 35, 357
Packard, N. H., et al. 1980, Phys. Rev. Lett., 45, 712
Rankin, J. M. 1983, ApJ, 274, 333
Romani, R. W., Rankin, J. M., & Backer, D. C. 1992, in IAU Colloq. 128, The Magnetospheric Structure and Emission Mechanisms of Radio Pulsars, ed. T. H. Hankins et al. (Zielona Gora, Poland: Pedagogical Univ. Press), 326
Ruelle, D. 1990, Proc. R. Soc. London A, 427, 241
Russell, D. A., & Ott, E. 1981, Phys. Fluids, 24, 1976
Shaw, R. 1981, Z. Naturforsch. A, 36, 80
———. 1984, The Dripping Faucet as a Model Chaotic System (Santa Cruz: Aeriel)
Takens, F. 1981, in Lecture Notes in Mathematics, Vol. 898, Dynamical Systems and Turbulence, ed. D. A. Rand & L.-S. Young (Berlin: Springer), 366
Theiler, J. 1988, Ph.D. thesis, California Inst. Tech.
Thorsett, S. E. 1991, ApJ, 377, 263
Thyagaraja, A. 1979, Phys. Fluids, 22, 2093
Weatherall, J. C. 1997, ApJ, 483, 402
———. 1998, ApJ, 506, 341
Wersinger, J.-M., Finn, J. M., & Ott, E. 1980a, Phys. Fluids, 23, 1142
———. 1980b, Phys. Rev. Lett., 44, 453
Wolf, A., et al. 1985, Physica D, 16, 285
Yuen, H. C., & Ferguson, W. E. 1978, Phys. Fluids, 21, 1275
Zakharov, V. E. 1972, Soviet Phys. JETP, 35, 908
Zhuravlev, V. I., & Popov, M. V. 1990, Soviet Astron., 34, 377